Quadrupolar-driven recoupling of homonuclear dipolar interactions in the nuclear magnetic resonance of rotating solids

Mattias Edén and Lucio Frydman[a)]
Department of Chemistry (M/C 111), University of Illinois at Chicago, 845 West Taylor Street, Room 4500, Chicago, Illinois 60607

(Received 18 October 2000; accepted 8 December 2000)

We discuss the recoupling of homonuclear dipolar interactions between quadrupolar nuclei under magic-angle spinning conditions, caused by the first-order quadrupolar interaction. This recoupling leads to NMR linewidths displaying a nonmonotonic dependence on the spinning frequency, meaning that broader lines may result as the spinning rate is increased. The effect depends on geometrical parameters of the spin system, which makes it suitable for distance measurements and for obtaining the relative orientations of dipolar and quadrupolar tensors. We propose a theoretical model of the dipolar recoupling based on average Hamiltonian theory, and find it in good agreement with numerically exact simulations and experiments on $I=3/2$ systems. © *2001 American Institute of Physics.* [DOI: 10.1063/1.1344886]

I. INTRODUCTION

Magic-angle spinning (MAS) NMR is used extensively as a tool for obtaining structural and dynamical information on a wide variety of solid systems. Combined with high power proton decoupling, MAS efficiently suppresses the effects from anisotropic interactions and allows one to obtain high resolution spectra on powders containing dilute spin-1/2 nuclei such as ^{13}C and ^{15}N. The averaging of MAS on spins-1/2 has been a topic of active research for several decades,[1–7] as has been the search for MAS techniques that selectively reintroduce certain spin interactions while suppressing others.[8–11] Particularly important in this regard has been the development of methods for recoupling the through-space dipolar interactions,[12,13] which can facilitate spectral assignment and convey distances and molecular geometries.

Similar developments stand at a less advanced stage in the area of NMR spectroscopy on quadrupolar nuclei. This is in part a consequence of the broad peaks that may arise even when detecting the central transition spectra of these spins, unaffected by the quadrupolar interaction to first order,[14] but not free of second-order quadrupolar effects. Yet the advent of new methods for obtaining high-resolution spectra of quadrupolar nuclei under MAS conditions[15,16] gives new relevance to investigating the nature of dipolar effects in such systems. Accordingly, attention has recently been given to analyses of the spectral broadening arising from dipolar couplings between half-integer quadrupolar nuclei.[17–24]

This article discusses some of the basic features of homonuclear interactions between quadrupolar nuclei undergoing MAS, and their effects on the NMR spectra. At first sight, dipolar effects on the central transitions of half-integer quadrupolar nuclei may not appear very different from their spin-1/2 counterparts, and one would expect that fast MAS should readily average them out. However, as is illustrated in Fig. 1, the noncommutation of quadrupolar and dipolar interactions leads to a quadrupolar-driven recoupling of homonuclear spin-pair dipolar interactions that persists even at very high spinning frequencies. The broadened central transition NMR line shapes resulting from this quadrupolar recoupling depend nonmonotonically on the spinning frequency, and the spectral features and broadenings are strongly dependent on the spin number I.

Duer *et al.* recently discussed homonuclear spin–spin interactions between quadrupolar nuclei[18,19] in the context of the MQMAS experiment.[25,26] More closely related to the effects presented in Fig. 1 is the recent work of Facey *et al.*[27,28] Here dipolar–quadrupolar correlations between two coupled deuterions were pointed out and analyzed in the limit of small quadrupolar couplings (relative to the spinning frequency) using average Hamiltonian theory (AHT). In several cases, however, the magnitudes of the quadrupolar frequencies are *not* small compared to the spinning frequency. Consequently, an alternative description is presented here. This theoretical model of the quadrupolar-driven recoupling is based on an average Hamiltonian treatment in the interaction frame of the quadrupolar interactions, and is valid for any spin number and for all ranges of MAS frequencies and quadrupolar couplings. We also investigate the quadrupolar-driven recoupling further by means of both numerically exact simulations and experimentally on half-integer quadrupolar nuclei, and observe results that are found in good general agreement with the analytical theory.

II. THEORY

A. The effective quadrupolar-driven recoupling hamiltonian

In order to elucidate the nature of the quadrupolar-driven recoupling, we consider two coupled quadrupolar nuclei j and k of spin I, undergoing MAS at the rotational frequency ω_r. For simplicity, we shall for the moment ignore J-couplings, chemical shift anisotropies, and second-order

a)Author to whom correspondence should be addressed. Electronic mail: lucio@uic.edu

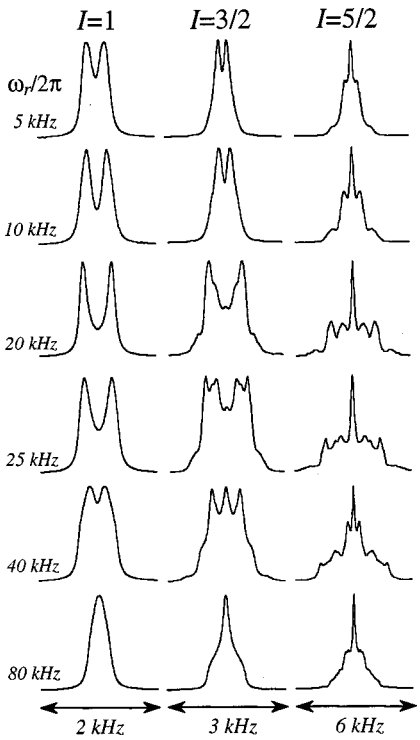

FIG. 1. Numerically exact simulations of the MAS line shapes expected for spin-pairs with spin number $I=1$ (left panel), 3/2 (middle), and 5/2 (right) at various spinning frequencies ω_r. All simulations employed a dipolar coupling $b_{jk}/2\pi=-1.0$ kHz and a quadrupolar frequency $\chi_Q/2\pi=33$ kHz (corresponding to quadrupole coupling constants $e^2qQ/h=66$, 200, and 666 kHz for $I=1$, 3/2, and 5/2, respectively). Axial quadrupolar tensors were assumed, placed perpendicular with respect to one another as well as to the direction of the dipolar vector. All spectra were convoluted with 100 Hz Lorentzian line-broadening, and in the absence of the dipolar coupling they show a sharp singlet. In the case $I=1$ the simulations employed stroboscopic sampling for ease of comparison: this provides line shapes free from first-order quadrupolar effects and with all transitions superimposed. Only the central transitions were calculated for the half-integer nuclei. The calculations were performed using the COMPUTE algorithm (Ref. 43), and 1154 ZCW (Refs. 44–46) orientations were used for powder averaging. On a 400 MHz Pentium computer, these simulations typically took 40 s, 2 min, and 20 min for $I=1$, $I=3/2$, and $I=5/2$, respectively.

quadrupolar interactions. For a single orientation in the powder, the high-field rotating-frame Hamiltonian is then

$$H(t)=H_{\rm iso}+H_Q^j(t)+H_Q^k(t)+H_D^{jk}(t). \tag{1}$$

Here $H_{\rm iso}$ contains the isotropic chemical shifts

$$H_{\rm iso}=\omega_j^{\rm iso}I_{jz}+\omega_k^{\rm iso}I_{kz}. \tag{2}$$

The dipolar and quadrupolar Hamiltonians are given by

$$H_D^{jk}(t)=\omega_{jk}(t)T_{20}^{jk}$$
$$=\frac{1}{\sqrt{6}}\omega_{jk}(t)\left(2I_{jz}I_{kz}-\frac{1}{2}I_j^+I_k^--\frac{1}{2}I_j^-I_k^+\right) \tag{3}$$

and

$$H_Q^p(t)=\omega_p^Q(t)T_{20}^p=\frac{1}{\sqrt{6}}\omega_p^Q(t)(3I_{pz}^2-I(I+1)),\quad p=j,k, \tag{4}$$

where T_{Lm} denotes the mth component of an Lth rank irreducible spherical tensor operator.[29] The dipolar frequency $\omega_{jk}(t)$ and the quadrupolar frequency $\omega_p^Q(t)$ are time-dependent due to the MAS modulation:

$$\omega_{jk}(t)=\sum_{n=-2}^{2}\omega_{jk}^{(n)}\exp\{in\omega_rt\}, \tag{5}$$

$$\omega_p^Q(t)=\sum_{n=-2}^{2}\omega_p^{(n)}\exp\{in\omega_rt\},\quad p=j,k. \tag{6}$$

These dipolar and quadrupolar frequencies are proportional to their respective coupling constants $b_{jk}=-\mu_0\hbar\gamma^2/4\pi r_{jk}^3$ and $\chi_Q=e^2qQ/2I(2I-1)\hbar$, where r_{jk} is the spin–spin internuclear distance and all other constants have their usual meaning. In terms of successive Wigner transformations,[29] the dipolar and quadrupolar Fourier coefficients in Eqs. (5) and (6) are given by

$$\omega_{jk}^{(n)}=\sqrt{6}b_{jk}\sum_{n'=-2}^{2}D_{0n'}^2(\Omega_{PM}^{jk})D_{n'n}^2(\Omega_{MR})d_{n0}^2(\beta_{RL}), \tag{7}$$

$$\omega_p^{(n)}=\sqrt{\frac{3}{2}}\sum_{n'',n'=-2}^{2}A_{2n''}^pD_{n''n'}^2(\Omega_{PM}^p)D_{n'n}^2(\Omega_{MR})d_{n0}^2(\beta_{RL}),$$
$$p=j,k. \tag{8}$$

Here the components of the quadrupolar tensors in their principal axis system (PAS) are given by $A_{20}^p=\chi_Q$, $A_{2\pm2}^p=-\chi_Q\eta_Q/\sqrt{6}$, $A_{2\pm1}^p=0$, and η_Q are their asymmetry parameters.[14] In these equations Ω_{PM} is a set of Euler angles specifying the transformation between the PAS of each NMR interaction and a reference frame fixed on the molecule. The transformation from this frame to one fixed on the rotor is given by the angles Ω_{MR}, which for a powdered sample are random. Finally, the z-axis of the rotor frame subtends an angle β_{RL} with respect to the static magnetic field direction; since magic-angle spinning is assumed throughout, $\beta_{RL}=\arctan\sqrt{2}$.

As the operators $I^\pm$ in H_D^{jk} do not commute with the longitudinal I_z^2-terms in H_p^Q, the Hamiltonian in Eq. (1) is time-dependent and not self-commuting. Consequently an exact analytical expression for the time-evolution of the spins cannot be found, and one must resort to approximations. One such possibility is offered by AHT,[30,4] which when applied to Eq. (1) over a rotational period $\tau_r=2\pi/\omega_r$ provides a time-independent effective Hamiltonian whose first two terms are[31]

$$\overline{H}^{(1)}=\tau_r^{-1}\int_0^{\tau_r}dt\,H(t), \tag{9}$$

$$\overline{H}^{(2)}=(i2\tau_r)^{-1}\int_0^{\tau_r}dt\int_0^t dt'\,[H(t),H(t')]. \tag{10}$$

This results in

$$\begin{aligned}\bar{H} &= H_{\mathrm{iso}} + 4\sum_{p=j,k} K_p[T_{20}^{jk}, T_{20}^{p}] \\ &= \omega_j^{\mathrm{iso}} I_{jz} + \omega_k^{\mathrm{iso}} I_{kz} + (K_j + K_k) I_j^+ I_k^- \\ &\quad + (K_j + K_k) I_j^- I_k^+ + 2K_j (I_j^+ I_k^- - I_j^- I_k^+) I_{jz} \\ &\quad - 2K_k (I_j^+ I_k^- - I_j^- I_k^+) I_{kz}, \end{aligned} \tag{11}$$

where

$$K_p = \frac{i}{2\omega_r} \sum_{n=1,2} n^{-1} \mathrm{Im}\{\omega_{jk}^{(n)} \omega_p^{(-n)}\}, \quad p = j,k. \tag{12}$$

Equation (11) is valid for arbitrary spin numbers I. An equivalent expression was recently given in terms of fictitious spin-1/2 operators for the case of two coupled $I=1$.[28] An analogous form was also derived by Maricq and Waugh for two coupled spins-1/2,[5] where they showed that noncommuting chemical shift anisotropies and dipolar couplings can lead to an $n=0$ ''rotational resonance'' recoupling.[32] Equation (11) can be considered as the quadrupolar analog of this effect, with the first-order quadrupolar interaction preventing the MAS averaging of the dipolar interaction and therefore leading to a line broadening proportional to $b_{jk}\chi_Q/\omega_r$.

The χ_Q/ω_r-type dependence of the linewidths predicted by Eq. (11) is in agreement with numerical simulations and experiments as long as $\chi_Q \ll \omega_r$. These conditions, however, comprise only a minority of systems; usually quadrupolar coupling constants fulfill $\chi_Q \geqslant \omega_r$, and it is thus a more complex linewidth dependence that is observed (e.g., Fig. 1). This breakdown of AHT stems from the fact that the quadrupolar couplings in Eq. (1) are actually larger than the modulation frequency ω_r. These large terms, however, may be removed from the Hamiltonian by transforming it into a quadrupolar interaction frame[33,22]

$$\tilde{H}(t) = U_Q(t,0)^\dagger H(t) U_Q(t,0) + i\frac{d}{dt} U_Q(t,0)^\dagger U_Q(t,0), \tag{13}$$

with

$$U_Q(t,0) = \exp\{-i\Phi_j^Q(t,0) T_{20}^j\} \exp\{-i\Phi_k^Q(t,0) T_{20}^k\}, \tag{14}$$

and the dynamic phases defined by $\Phi_p^Q(t,0) = \int_0^t \omega_p^Q(t')dt'$, $p=j,k$. These phases are related to the quadrupolar Fourier coefficients of Eq. (8) by

$$\Phi_p^Q(t,0) = (i\omega_r)^{-1} \sum_{n\neq 0} n^{-1} \omega_p^{(n)} (\exp\{in\omega_r t\} - 1). \tag{15}$$

As the chemical shifts and the $I_{jz}I_{kz}$ term of the dipolar interaction commute with $U_Q(t,0)$, the interaction frame Hamiltonian may be written as

$$\tilde{H}(t) = H_{\mathrm{iso}} + \sqrt{\tfrac{2}{3}}\,\omega_{jk}(t) I_{jz} I_{kz} + \tilde{H}_D^{jk}(t). \tag{16}$$

The ''interesting'' dynamics here are contained in $\tilde{H}_D^{jk}(t)$, the flip-flop part of the dipolar Hamiltonian. By identifying in Eq. (3) $-\frac{1}{2}(I_j^+ I_k^- + I_j^- I_k^+) = T_{11}^j T_{1-1}^k + T_{1-1}^j T_{11}^k$, this noncommuting term may be expressed as

$$\tilde{H}_D^{jk}(t) = \frac{1}{\sqrt{6}}\,\omega_{jk}(t) U_Q(t,0)^\dagger (T_{11}^j T_{1-1}^k + T_{1-1}^j T_{11}^k) U_Q(t,0). \tag{17}$$

The time-dependence imposed on the $T_{1m}^j T_{1-m}^k$ terms by $U_Q(t,0)$ may be derived from the results of Bowden *et al.*[34,35]

$$U_Q(t,0)^\dagger T_{1m}^j T_{1-m}^k U_Q(t,0) = \sum_{L_j, L_k=1}^{2I} Q_{L_jL_k}(t) T_{L_jm}^j T_{L_k-m}^k. \tag{18}$$

Here the $Q_{L_jL_k}(t)$ terms are given by products of oscillatory functions of the quadrupolar phases $\exp\{iC_I\Phi_p^Q(t,0)\}$, where the constant C_I depends on the spin number: $C_I = \sqrt{\frac{3}{2}}$ for integer spins and $C_I = \sqrt{6}$ for half-integer spins. Since the quadrupolar couplings are themselves oscillating at frequencies $\pm\omega_r$ and $\pm 2\omega_r$, the functions $\exp\{iC_I\Phi_p^Q(t,0)\}$ may be written as infinite Fourier–Bessel series with base frequency ω_r:[32]

$$\exp\{iC_I\Phi_\Lambda^Q(t,0)\} = \sum_{n=-\infty}^{\infty} a_\Lambda^{(n)} \exp\{in\omega_r t\}, \quad \Lambda = j,k,\Sigma,\Delta. \tag{19}$$

Contributions to the $a_\Lambda^{(n)}$ coefficients arise from the phases accumulated by the individual quadrupolar frequencies $\Phi_p^Q(t,0)$, as well as from their sum $\Phi_\Sigma^Q(t,0) = \Phi_j^Q(t,0) + \Phi_k^Q(t,0)$, and difference $\Phi_\Delta^Q(t,0) = \Phi_j^Q(t,0) - \Phi_k^Q(t,0)$. The interaction frame dipolar Hamiltonian in Eq. (17) may be cast as

$$\begin{aligned}\tilde{H}_D^{jk}(t) = \frac{1}{\sqrt{6}}\,\omega_{jk}(t) \sum_{L_j, L_k=1}^{2I} Q_{L_jL_k}(t) \{ & T_{L_j1}^j T_{L_k-1}^k \\ & + (-1)^{L_j - L_k} T_{L_j-1}^j T_{L_k1}^k \}, \end{aligned} \tag{20}$$

where the functions $Q_{L_jL_k}(t)$ are given by

$$Q_{L_jL_k}(t) = \sum_{n=-\infty}^{\infty} Q_{L_jL_k}^{(n)} \exp\{in\omega_r t\}. \tag{21}$$

It follows that $\tilde{H}_D^{jk}(t)$ is given by the product of two time-dependent terms: the dipolar coupling $\omega_{jk}(t)$ modulated at frequencies $\pm\omega_r$ and $\pm 2\omega_r$ by the action of MAS, and the functions $Q_{L_jL_k}(t)$ that are modulated at frequencies $n\omega_r$ ($n=0,\pm 1,\pm 2,...$) due to the time-dependence imposed on the spin parts of the Hamiltonian by the transformation operator $U_Q(t,0)$. Equation (20) thus conveys the basic mechanism of the quadrupolar-driven dipolar recoupling: recoupling occurs because the time-dependence of $Q_{L_jL_k}(t)$ cancels the MAS modulation of $\omega_{jk}(t)$. This idea can be exploited further to derive an explicit recoupling Hamiltonian. Since the phases $\Phi_p^Q(t,0)$ refocus over one rotational period [$U_Q(\tau_r,0)=1$], and $\tilde{H}_D^{jk}(t)$ is periodic [$\tilde{H}_D^{jk}(t+\tau_r) = \tilde{H}_D^{jk}(t)$], the application of AHT in the interaction frame is suitable. Taking the average of Eq. (16) over one rotational period then gives

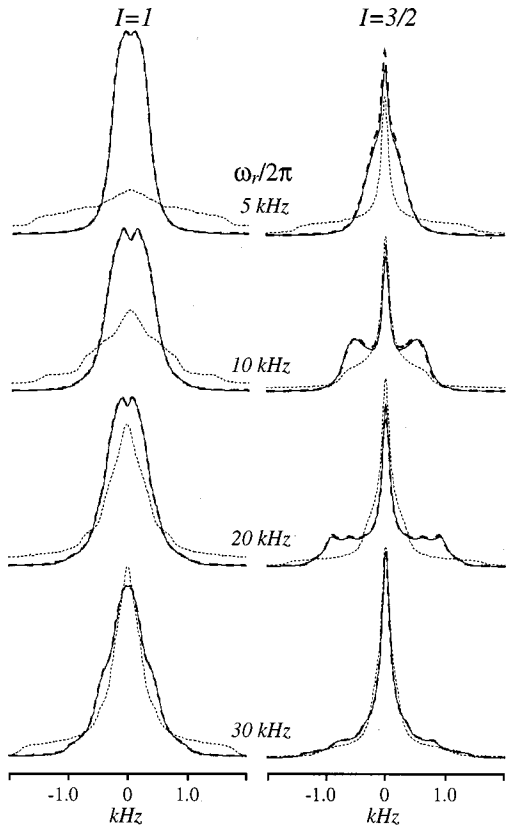

FIG. 2. Comparisons between numerically exact simulations of the quadrupolar-driven recoupling (solid lines) and line shapes obtained from two AHT treatments: Eq. (22) (dashed lines) and Eq. (11) (dotted lines). Left panel: Spectra obtained for $I=1$, with $\chi_Q/2\pi=40$ kHz and $\eta_Q=0.5$. The tensors were oriented such that $\Omega_{PM}^{jk}=(0,0,0)$, $\Omega_{PM}^{j}=(0,\pi/3,0)$, and $\Omega_{PM}^{k}=(0,\pi/3,\pi/6)$. Right panel: Central transition spectra obtained for $I=3/2$, with $\chi_Q/2\pi=20$ kHz, $\eta_Q=0$, $\Omega_{PM}^{jk}=(0,0,0)$, $\Omega_{PM}^{j}=\Omega_{PM}^{k}=(0,\pi/2,0)$. Other calculation parameters are as in Fig. 1. Some of the traces stemming from Eq. (11) (particularly those for $I=1$) have been truncated for presentation purposes.

$$\bar{H}^{(1)}=H_{\mathrm{iso}}+\frac{1}{\sqrt{6}}\sum_{L_j,L_k=1}^{2I}\sum_{n=-2}^{2}\omega_{jk}^{(n)}Q_{L_jL_k}^{(-n)}\{T_{L_j1}^{j}T_{L_k-1}^{k}+(-1)^{L_j-L_k}T_{L_j-1}^{j}T_{L_k1}^{k}\}. \tag{22}$$

From these equations, analytical expressions of the recoupled dipolar Hamiltonian can be derived for any spin number I. Explicit expressions for the cases $I=1$ and $I=3/2$ are given in the Appendix.

Figure 2 compares a series of MAS spectra resulting from powder averages of these interaction-frame AHT expressions with numerically exact simulations for various spinning frequencies. The spectra obtained from the Hamiltonian in Eq. (11) are also shown for comparison. As expected, good agreement is only obtained in this latter case when $\chi_Q<\omega_r$. By contrast, the interaction-frame average Hamiltonian from Eq. (22) describes the quadrupolar-driven recoupling over the entire range of χ_Q/ω_r values, as its derivation only requires that the dipolar coupling be much smaller than ω_r and than the various quadrupolar frequencies. Furthermore, as will be described in more detail elsewhere, when such conditions are not met the Fourier coefficients in Eqs. (19) and (21) may be used to derive the necessary higher-order Magnus correction terms.

B. A physical interpretation of the recoupling

Despite the abstract nature of the analytical expressions above, this AHT treatment provides qualitative insight into the dependence of the quadrupolar-driven dipolar recoupling on the spinning frequency. Since the interaction-frame dipolar Hamiltonian is proportional to $\{Q^{(n)}\}$ [Eq. (21)], which in turn depend on $\{a_\Lambda^{(n)}\}$ [Eq. (19)], the extent of the recoupling will depend on the magnitudes of these coefficients. The $\{a_\Lambda^{(n)}\}$ set of coefficients originates from the time-evolution operator of the first-order quadrupolar coupling, and in physical terms $a_\Lambda^{(n)}$ represents the amplitude of the nth order sideband in the MAS spectrum generated by the quadrupolar interactions (as well as by the sum and difference of the quadrupolar frequencies of the two sites). Furthermore, Eq. (22) shows that to first order in AHT only the amplitudes of the first- and second-order sidebands contribute to the recoupling. As is well-known,[5] the amplitudes of these MAS sidebands depend on the ratio between the magnitude of the NMR interaction and the spinning frequency, i.e., on χ_Q/ω_r. For small values of χ_Q/ω_r all intensity is concentrated at the centerband, whereas for large values of χ_Q/ω_r the total intensity is distributed over a large number of (weak) sidebands. In either of these cases, Eq. (22) predicts that the dipolar recoupling effects are relatively small. By contrast, when $\chi_Q/\omega_r\simeq 1$, the first- and second-order sidebands of the quadrupolar effects have their highest intensities, leading to the most efficient recoupling and to the largest line-broadening. Although somewhat simplistic, this picture implies that the quadrupolar-induced dipolar linewidth for a homonuclear spin-pair passes over a maximum when the spinning frequency is about the size of the quadrupolar frequencies. Since quadrupolar frequencies are generally large (10^1-10^4 kHz) and modern MAS frequencies are in the order of 10^1 kHz, the quadrupolar-driven recoupling will not be maximized for most spin systems. Therefore in a majority of cases, peak widths can be expected to *increase* as ω_r increases. This runs counter to common experience in solid-state NMR, where increasing the spinning frequency normally leads to a *decrease* in the linewidths. However, such nonmonotonic recoupling behavior has been reported in homonuclear spin–pairs with $I=1/2$ (Ref. 36) and predicted for $I=1$ (Ref. 37) using a theoretical treatment similar to that given here. The following section gives preliminary examples of this unusual behavior in the quadrupolar-driven recoupling of homonuclear systems.

III. EXPERIMENTAL RESULTS

In order to test our theoretical predictions, experimental MAS NMR spectra from powders of various inorganic compounds containing the $I=3/2$ nuclei ^{7}Li, ^{23}Na, and ^{79}Br were recorded. These salts were chosen mainly for their sizable and/or numerous homonuclear dipolar couplings, estimated from x-ray data[38–42] as $b_{jk}/2\pi=-550$ Hz ($Li_2SO_4\cdot H_2O$), -1100 Hz ($LiOH\cdot H_2O$), -460 Hz ($Li_2C_2O_4$), -140 Hz (NaCl), and -80 Hz (KBr). All

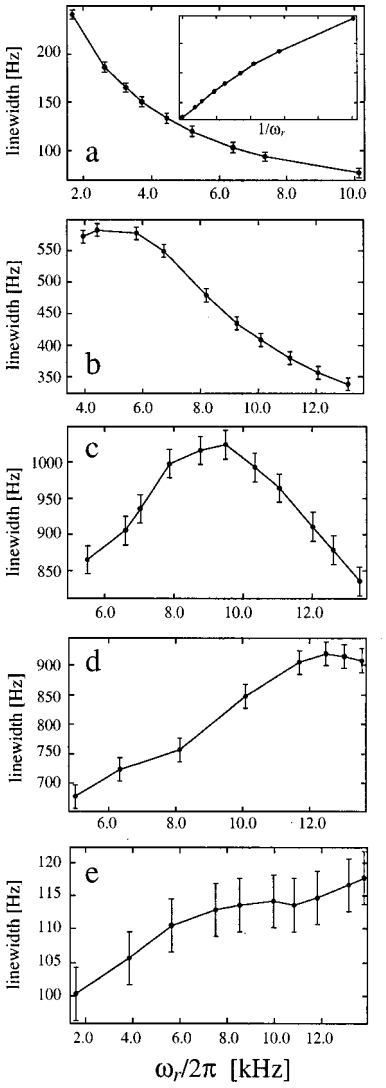

FIG. 3. Experimental central transition spectral linewidths (full widths at half height) as a function of spinning frequency for five powders containing various $I=3/2$ nuclei (^{7}Li, ^{23}Na, and ^{79}Br): (a) NaCl, (b) $Li_2SO_4\cdot H_2O$, (c) $LiOH\cdot H_2O$, (d) $Li_2C_2O_4$, and (e) KBr. The linewidths were obtained by fittings to Lorentzian shapes, and the error bars represent the linewidth uncertainties resulting from repeated NMR measurements. The inset in (a) plots the ^{23}Na linewidth as function of $1/\omega_r$.

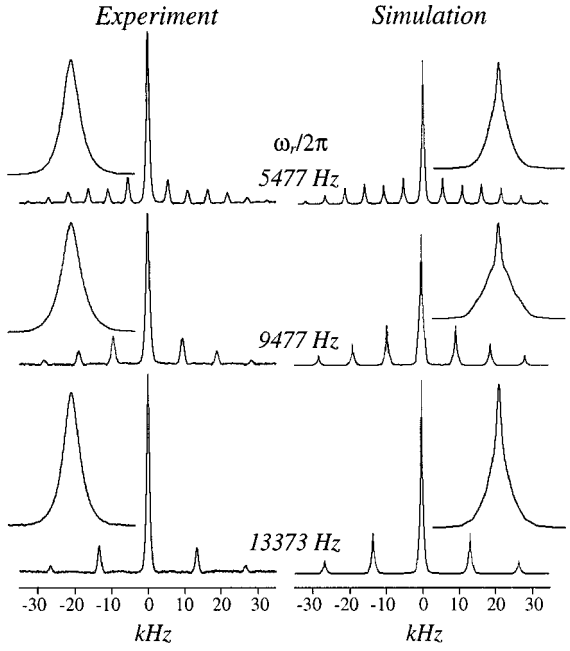

FIG. 4. Comparison between the experimental spectra (left panel) of lithium hydroxide monohydrate [Fig. 3(c)] and numerically exact spin-pair simulations (right panel) for three spinning frequencies: $\omega_r/2\pi=5477$ Hz, 9477 Hz, and 13373 Hz. The simulations assumed the following parameters: $b_{jk}/2\pi=-1.1$ kHz, $\chi_Q/2\pi=10.8$ kHz, $\eta_Q=0.70$, $\Omega^{jk}_{PM}=(0,0,0)$, $\Omega^{j}_{PM}=\Omega^{k}_{PM}=(0,\pi/3,0)$, $\omega_0/2\pi=-117$ MHz, and line-broadening 250 Hz. The magnified centerband is shown for each spectrum.

compounds were purchased from Aldrich, and used after recrystallization. The spectra were recorded on a homebuilt spectrometer at 7.1 T, using a commercial 4 mm Bruker probe and single-pulse excitation. For the samples containing protons, high-power ^{1}H decoupling was employed. Attention was paid to the central transition linewidths as function of the spinning frequency.

Figure 3(a) shows the ^{23}Na linewidth in NaCl as function of ω_r. This compound has negligible electrical field gradients; the quadrupolar-driven recoupling is then essentially nonexistent, and as predicted by Eq. (11) the peak narrows monotonically as ω_r increases. A similar behavior is found for the ^{7}Li NMR linewidth in $Li_2SO_4\cdot H_2O$ [Fig. 3(b)], which according to its satellite sideband intensities has a small quadrupolar frequency of 8.3 kHz. The situation is different, however, for the MAS NMR ^{7}Li linewidth in $LiOH\cdot H_2O$ [Fig. 3(c)]: the quadrupolar frequency here is 10.8 kHz, and the AHT treatment presented above predicts a maximum linewidth when $\omega_r/2\pi$ is around 7.0–10.0 kHz. This agrees well with the experimental results where $\omega_r/2\pi \approx 9.4$ kHz ($\chi_Q/\omega_r=1.2$) gave the broadest line. Finally, Figs. 3(d) and 3(e) exemplify the typical situation encountered when $\chi_Q > \omega_r$. Fitting the satellite transition spectra for these compounds gave the quadrupolar frequencies $\chi_Q/2\pi=16.7$ kHz ($Li_2SO_4\cdot H_2O$) and 25 kHz (KBr). For $Li_2SO_4\cdot H_2O$, the maximum linewidth is found around 12.5 kHz ($\chi_Q/\omega_r=1.3$); for KBr the χ_Q/ω_r ratio corresponding to the maximum linewidth cannot be reached within our range of spinning frequencies and the line becomes broader as the spinning frequency is increased.

The nonmonotonic dependence of the linewidth on the spinning speed is seen most clearly for $LiOH\cdot H_2O$. Figure 4 compares an experimental set of MAS spectra obtained on this compound against numerically exact two-spin simulations. This set of spectra further reveals how the central transition linewidths relate to the sideband structure from the satellite transitions: in accordance with theory, the broadest line is obtained when the absolute intensities of the first- and second-order sidebands are maximized. Numerical simulations (right panel of Fig. 4) reproduce well this overall experimental trend, especially when considering that only a single dipolar coupling and arbitrary orientations were assumed for describing such a complex multispin lattice.

IV. ADDITIONAL CONSIDERATIONS

As mentioned above, the actual extent of the dipolar recoupling depends on the sums and differences of the qua-

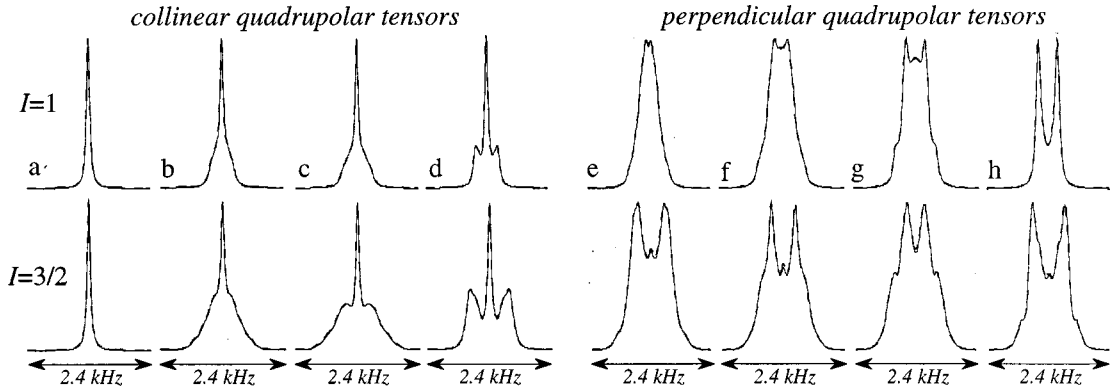

FIG. 5. Simulated MAS line shapes for a homonuclear pair with spin number $I=1$ (top traces) and 3/2 (lower traces) for various relative orientations of the dipolar and quadrupolar interactions. All simulations employed $\omega_r/2\pi=25.0$ kHz, $b_{jk}/2\pi=-750$ Hz, $\eta_Q=0$, $\chi_Q/2\pi=41.25$ kHz (corresponding to quadrupole coupling constants $e^2qQ/h=82.5$ kHz and 250 kHz for $I=1$ and 3/2, respectively), and 75 Hz Lorentzian line-broadening. The dashed lines are AHT calculations using Eq. (22). These are almost indistinguishable from numerically exact simulations (solid lines). Spectra (a)–(d) show the line shape dependence for various relative orientations between the dipolar and quadrupolar tensors (for collinear quadrupolar tensors), (e)–(h) shows the dependence when changing the relative orientations between the two quadrupolar tensors (in the case of perpendicular dipolar and quadrupolar tensors). The dipolar tensor was fixed at $\Omega_{PM}^{jk}=(0,0,0)$ and the Euler angles for the collinear quadrupolar orientations ($\Omega_{PM}^{j}=\Omega_{PM}^{k}$) were (a) (0,0,0), (b) $(0,\pi/6,0)$, (c) $(0,\pi/3,0)$, (d) $(0,\pi/2,0)$. For (e)–(h), $\Omega_{PM}^{j}=(0,\pi/2,0)$ was fixed, and Ω_{PM}^{k} was changed according to (e) $(0,\pi/2,\pi/9)$, (f) $(0,\pi/2,2\pi/9)$, (g) $(0,\pi/2,\pi/3)$, and (h) $(0,\pi/2,\pi/2)$.

drupolar frequencies involved. Hence it will be a function of both the coupling constants of each site, as well as the relative orientations between these tensors. Furthermore if all anisotropies in Eq. (1) are axial and collinear, their spatial components can be factored out; the total Hamiltonian then commutes with itself at different points in time, and the recoupling ceases regardless of the values of the coupling constants. Figure 5 summarizes some of these orientation-dependent considerations, illustrating line shapes that can be expected for identical sets of quadrupolar coupling parameters, but different relative tensor orientations. These plots also evidence an increase in the effective recoupling strength as the quadrupolar tensors become noncoincident, as pointed out in Ref. 28. The plots also yield an additional proof for the excellent agreement between the predictions of the analytical and numerical methods.

So far we have been concerned with spin systems affected solely by first-order quadrupolar and dipolar effects, as in this case the nature of the recoupling is most easily understood and its consequences most evident. The quadrupolar-driven recoupling, however, will also be strongly affected by field-dependent effects, including chemical shifts and second-order quadrupolar interactions. Neither of these interactions commute with the dipolar flip-flop terms, and they will generally truncate the effects from the dipolar coupling.[18,19] The quadrupolar-driven recoupling is therefore most prominent for spins with equal isotropic chemical shifts, relatively small quadrupolar coupling constants, and large Larmor frequencies.

An idea of the truncating effects that can be expected from quadrupolar and chemical shift effects is conveyed in Fig. 6. In the case of large second-order quadrupolar effects, the dipolar broadening of MAS line shapes is typically small compared with the second-order broadenings themselves. Yet as shown by Figs. 6(a) and 6(b) the dipolar couplings may still distort the second-order line shapes significantly, thus affecting the accuracy with which quadrupolar parameters can be extracted by fitting of experimental line shapes if homonuclear couplings are neglected. The dependence of the recoupling on the relative orientations between the various tensors involved is again evident from these plots. Furthermore, since the second-order quadrupolar dispersion scales inversely with the Larmor frequency, the effects of the quadrupolar-driven recoupling can be expected to grow as the static magnetic field increases.

As for isotropic chemical shifts, numerical simulations and experiments demonstrate that even small shift differences between the spins markedly attenuate the recoupling. The truncating effects of isotropic chemical shifts on the quadrupolar-driven recoupling are exemplified in Figs. 6(c)–6(f). In this respect, the behavior displayed by quadrupolar spins is similar to that of coupled spin-1/2 nuclei.[32] Simulations indicate that anisotropic chemical shifts also interfere with the quadrupolar-driven recoupling, particularly if they are substantially larger than the dipolar coupling (data not shown). Yet homonuclear dipolar interactions as well as quadrupolar-driven effects become again significant at rotational resonance conditions. A more detailed analysis on the effects of the quadrupolar-driven recoupling at rotational resonance will be reported elsewhere.

As the MQMAS experiment[25,26] has become a most widely used technique for obtaining high-resolution spectra of quadrupolar nuclei, it is also worth referring to how quadrupolar-driven recoupling phenomena affect it. From numerical simulations and experiments (not shown), it follows that the quadrupolar-driven recoupling has different impact on the various transitions of the spin system. Broadening effects from the quadrupolar-driven recoupling seem much less pronounced in the isotropic dimension of an MQMAS spectrum than in its anisotropic dimension. Therefore it appears that from a resolution standpoint, the MQMAS technique successfully suppresses most of these homonuclear dipolar effects.

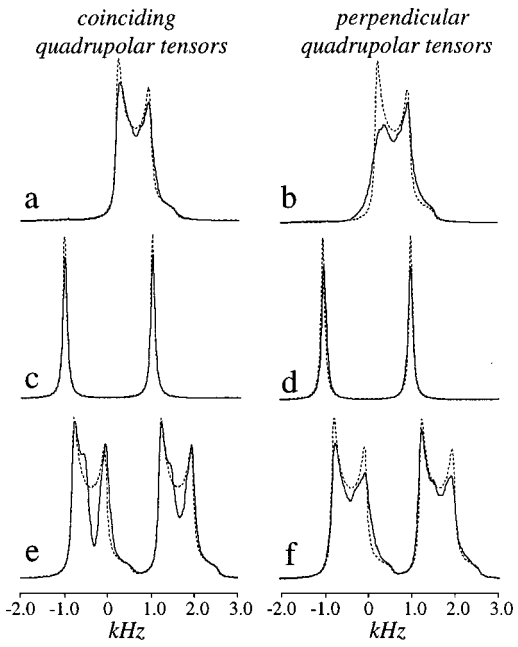

FIG. 6. Effects of isotropic chemical shifts and second-order quadrupolar interactions on the quadrupolar-driven recoupling. These numerically exact MAS simulations assumed two $I=3/2$ with $\chi_Q/2\pi=333$ kHz and $\eta_Q=0$ at $\omega_r/2\pi=20$ kHz. Dotted lines: no dipolar couplings. Solid lines: using $b_{jk}/2\pi=-2.0$ kHz. The simulations on the left panel (a), (c), (e) assumed parallel quadrupolar tensors, while those on the right panel (b), (d), (f) used perpendicular tensors. In all cases the quadrupolar tensors were perpendicular to the dipolar vector. (a), (b) Dipolar effects in the presence of second-order quadrupolar interactions ($\omega_0/2\pi=-160$ MHz) for two spins with equal chemical shifts. (c), (d) Two spins with a shift separation of 2 kHz, but without second-order quadrupolar effects. (e), (f) Same as (c), (d), but including the second-order quadrupolar interactions ($\omega_0/2\pi=-160$ MHz).

V. CONCLUSIONS

This work investigated how the presence of quadrupolar interactions may interfere with the MAS averaging of homonuclear dipolar couplings between quadrupolar nuclei. This effect is unusual in that it enables first-order quadrupolar interactions, which do not affect symmetric $-m\leftrightarrow m$ transitions, to result in broadened central transition MAS spectra via a dipolar recoupling. The extent of the quadrupolar-driven dipolar recoupling depends on several factors: (i) the magnitudes of the quadrupolar frequencies relative to the spinning frequency, (ii) the relative orientations between the dipolar and quadrupolar tensors, (iii) the relative orientations between the two quadrupolar tensors, (iv) the spin number of the nuclei, and (v) the presence of chemical shifts and second-order quadrupolar interactions. We have shown that all of these effects can be accounted for either numerically, or analytically by a quadrupolar interaction-frame AHT treatment.

In many cases the dipolar effects being discussed here are too small to cause a significant line broadening of the spectral peaks, but may still be exploited in magnetization-transfer experiments among homonuclear systems of quadrupolar nuclei. In fact the strong dependence of the quadrupolar-driven recoupling on geometrical parameters may enable its use for distance measurements, for determinations of the relative orientations between the dipolar and quadrupolar tensors, as well as between the quadrupolar tensors themselves. Quadrupolar-driven recoupling effects will also play a significant role when attempting to adapt existing spin-1/2 methods of homonuclear recoupling to quadrupolar nuclei.

From a spectroscopic point of view, the most unusual feature of these recoupling effects is probably their enhancement with increasing spinning rates. Yet similar concepts apply to a wide variety of recoupling phenomena, including spin diffusion between isolated spin-1/2 pairs as well as line broadening effects in systems of strongly-coupled spin-1/2 nuclei.[36] A generalization of the theory given here to such systems will be given elsewhere.

TABLE I. Explicit expressions for $\bar{\omega}_{L_jL_k}$, $\{L_j,L_k\}=\{1,2\}$ for $I=1$.

$\{L_j,L_k\}$	1	2
1	$F_\Sigma^+ + F_\Delta^+$	$-\sqrt{2}(F_\Sigma^- - F_\Delta^-)$
2	$\sqrt{2}(F_\Sigma^- + F_\Delta^-)$	$-2(F_\Sigma^+ - F_\Delta^+)$

ACKNOWLEDGMENTS

We would like to thank V. Frydman for assistance in choosing and recrystallizing the samples, and C. V. Grant for discussions. This work was supported by the NSF through Grants DMR-986810 and CHE-9841790 (Creativity Extension Award), and by the DOE through Grant 00ER15049. L. F. is a Camille Dreyfus Teacher–Scholar, University of Illinois Junior Scholar, and Alfred P. Sloan fellow. M. E. acknowledges a post-doctoral fellowship from The Swedish Foundation for International Cooperation in Research and Higher Education (STINT). This work was presented in part at the 42nd Rocky Mountain Conference, Poster 273, (Broomfield, Colorado, August 2000).

TABLE II. Explicit expressions for $\bar{\omega}_{L_jL_k}$, $\{L_j,L_k\}=\{1,2,3\}$ for $I=3/2$.

$\{L_j,L_k\}$	1	2	3
1	$\frac{3}{25}\{3(F_\Sigma^+ + F_\Delta^+)+4(F_j^+ + F_k^+)\}$	$-\frac{1}{5\sqrt{2}}\{3(F_\Sigma^- - F_\Delta^-)+4F_k^-\}$	$\frac{2}{5\sqrt{15}}\{3(F_\Sigma^+ + F_\Delta^+)-6F_j^+ + 4F_k^+\}$
2	$\frac{1}{5\sqrt{2}}\{3(F_\Sigma^- + F_\Delta^-)+4F_j^-\}$	$-\frac{1}{2}(F_\Sigma^+ - F_\Delta^+)$	$\sqrt{\frac{2}{15}}(F_\Sigma^- + F_\Delta^- - 2F_j^-)$
3	$\frac{2}{5\sqrt{15}}\{3(F_\Sigma^+ + F_\Delta^+)+4F_j^+ - 6F_k^+\}$	$\sqrt{\frac{2}{15}}(-F_\Sigma^- + F_\Delta^- + 2F_k^-)$	$\frac{4}{15}\{F_\Sigma^+ + F_\Delta^+ - 2(F_j^+ + F_k^+)\}$

APPENDIX

Here we present expressions for the quadrupolar-driven dipolar recoupling Hamiltonian for the cases $I=1$ and $I=3/2$. It follows from Eq. (17) that the first-order average Hamiltonian may be written as

$$\overline{H}=H_{\mathrm{iso}}+\sum_{L_j,L_k=1}^{2I}\overline{\omega}_{L_jL_k}\{T^j_{L_j1}T^k_{L_k-1}+(-1)^{L_j-L_k}T^j_{L_j-1}T^k_{L_k1}\},\tag{A1}$$

with

$$\overline{\omega}_{L_jL_k}=\frac{1}{\sqrt{6}}\sum_{n=-2}^{2}\omega^{(n)}_{jk}Q^{(-n)}_{L_jL_k}.\tag{A2}$$

The coefficients $\overline{\omega}_{L_jL_k}$ in Eq. (A2) may be described in terms of the functions

$$F^{\pm}_{\Lambda}=\frac{1}{4\sqrt{6}}\sum_{n=-2}^{2}\omega^{(n)}_{jk}\{a^{(-n)}_{\Lambda}\pm a^{(n)*}_{\Lambda}\},\quad \Lambda=j,k,\Sigma,\Delta,\tag{A3}$$

where $a^{(n)}_{\Lambda}$ is given by Eq. (19). Explicit expressions of the $\{\overline{\omega}_{L_jL_k}\}$ sets for $I=1$ and $I=3/2$ are given in Tables I and II. When combined with the irreducible spherical tensors,

$$T_{1\pm1}=\mp\frac{1}{\sqrt{2}}I^{\pm},\tag{A4}$$

$$T_{2\pm1}=\mp\tfrac{1}{2}I^{\pm}(2I_z\pm1),\tag{A5}$$

$$T_{3\pm1}=\mp\sqrt{\tfrac{3}{4}}I^{\pm}\{5(I_z^2\pm I_z)+I(I+1)+2)\},\tag{A6}$$

these can be used to derive the average Hamiltonians in terms of spin product operators. For instance when $I=1$ one has

$$\begin{aligned}\overline{H}=&\omega^{\mathrm{iso}}_jI_{jz}+\omega^{\mathrm{iso}}_kI_{kz}-(F^+_{\Sigma}-F^-_{\Sigma})I^+_jI^-_k-(F^+_{\Sigma}-F^-_{\Sigma})\\&\times I^-_jI^+_k-G^+(I^+_jI^-_k-I^-_jI^+_k)I_{jz}\\&+G^-(I^+_jI^-_k-I^-_jI^+_k)I_{kz}+2(F^+_{\Sigma}-F^+_{\Delta})\\&\times(I^+_jI^-_k+I^-_jI^+_k)I_{jz}I_{kz},\end{aligned}\tag{A7}$$

where $G^{\pm}=(F^+_{\Sigma}+F^-_{\Sigma}-F^+_{\Delta}\pm F^-_{\Delta})$.

[1] E. R. Andrew, A. Bradbury, and R. G. Eades, Nature (London) **183**, 1802 (1959).
[2] I. J. Lowe, Phys. Rev. Lett. **2**, 285 (1959).
[3] J. Schaefer and E. O. Stejskal, J. Am. Chem. Soc. **98**, 1031 (1976).
[4] U. Haeberlen, in *High Resolution NMR in Solids. Selective Averaging*, edited by J. S. Waugh (Academic, New York, 1976).
[5] M. M. Maricq and J. S. Waugh, J. Chem. Phys. **70**, 3300 (1979).
[6] S. Ray, E. Vinogradov, G.-J. Boender, and S. Vega, J. Magn. Reson. **135**, 418 (1998).
[7] C. Filip, S. Hafner, I. Schnell, D. E. Demco, and H. W. Spiess, J. Chem. Phys. **110**, 423 (1999).
[8] R. Tycko, G. Dabbagh, and P. A. Mirau, J. Magn. Reson. **85**, 265 (1989).
[9] T. Gullion and J. Schaefer, Adv. Magn. Reson. **13**, 57 (1989).
[10] M. Hohwy and N. C. Nielsen, J. Chem. Phys. **109**, 3780 (1998).
[11] M. Carravetta, M. Edén, X. Zhao, A. Brinkmann, and M. H. Levitt, Chem. Phys. Lett. **321**, 205 (2000).
[12] A. E. Bennett, R. G. Griffin, and S. Vega, NMR Basic Principles and Progress **33**, 1–77 (1994).
[13] S. Dusold and A. Sebald, Annu. Rep. NMR Spectrosc. **41**, 185 (2000).
[14] A. J. Vega, in *Encyclopedia of NMR*, edited by D. M. Grant and R. K. Harris (Wiley, New York, 1995), pp. 3869–3888.
[15] B. F. Chmelka and J. W. Zwanziger, NMR Basic Principles and Progress **33**, 80 (1994).
[16] M. E. Smith and E. R. H. van Eck, Prog. Nucl. Magn. Reson. Spectrosc. **34**, 159 (1999).
[17] Y. Wu, Z.-Y. Peng, B. Q. Sun, and A. Pines, J. Magn. Reson., Ser. A **102**, 29 (1993).
[18] M. J. Duer, Chem. Phys. Lett. **277**, 167 (1997).
[19] M. J. Duer and A. J. Painter, Chem. Phys. Lett. **313**, 763 (1999).
[20] J. McManus, R. Kemp-Harper, and S. Wimperis, Chem. Phys. Lett. **311**, 292 (1999).
[21] G. Wu and K. Yamada, Chem. Phys. Lett. **313**, 519 (1999).
[22] M. Baldus, D. Rovnyak, and R. G. Griffin, J. Chem. Phys. **112**, 5902 (2000).
[23] M. Nijman, M. Ernst, A. P. Kentgens, and B. H. Meier, Mol. Phys. **98**, 161 (2000).
[24] S. Wi and L. Frydman, J. Chem. Phys. **112**, 3248 (2000).
[25] L. Frydman and J. S. Harwood, J. Am. Chem. Soc. **117**, 5367 (1995).
[26] A. Medek, J. S. Harwood, and L. Frydman, J. Am. Chem. Soc. **117**, 12779 (1995).
[27] G. Facey, T. P. Fong, D. Gusev, P. M. McDonald, R. H. Morris, M. Schlaf, and W. Xu, Can. J. Chem. **77**, 1899 (1999).
[28] G. Facey, D. Gusev, R. H. Morris, S. Macholl, and G. Buntkowsky, Phys. Chem. Chem. Phys. **2**, 935 (2000).
[29] D. A. Varshalovich, A. N. Moskalev, and V. K. Khersonskii, *Quantum Theory of Angular Momentum* (World Scientific, Singapore, 1988).
[30] U. Haeberlen and J. S. Waugh, Phys. Rev. **175**, 453 (1968).
[31] W. Magnus, Commun. Pure Appl. Math. **7**, 649 (1954).
[32] M. H. Levitt, D. P. Raleigh, F. Creuzet, and R. G. Griffin, J. Chem. Phys. **90**, 6347 (1990).
[33] W. Sun, J. T. Stephen, L. D. Potter, and Y. Wu, J. Magn. Reson., Ser. A **116**, 181 (1995).
[34] G. J. Bowden and W. D. Hutchison, J. Magn. Reson. **67**, 403 (1986).
[35] G. J. Bowden, W. D. Hutchison, and J. Khachan, J. Magn. Reson. **67**, 415 (1986).
[36] A. Kubo and C. A. McDowell, J. Chem. Phys. **92**, 7156 (1990).
[37] Z. Gan and P. Robyr, Mol. Phys. **95**, 1143 (1998).
[38] *Gmelin Handbook of Inorganic and Organometallic Chemistry* (Springer-Verlag, Berlin, 1952), Vol. 21, p. 310.
[39] *Gmelin Handbook of Inorganic and Organometallic Chemistry* (Springer-Verlag, Berlin, 1952), Vol. 22, p. 519.
[40] B. Beagley and R. W. H. Small, Acta Crystallogr. **17**, 783 (1964).
[41] A. C. Larson, Acta Crystallogr. **17**, 783 (1965).
[42] N. W. Alcock, Acta Crystallogr., Sect. B: Struct. Crystallogr. Cryst. Chem. **27**, 1682 (1971).
[43] M. Edén, Y. K. Lee, and M. H. Levitt, J. Magn. Reson., Ser. A **120**, 56 (1996).
[44] S. K. Zaremba, Ann. Mat. Pura. Appl. **4:73**, 293 (1966).
[45] H. Conroy, J. Chem. Phys. **47**, 5307 (1967).
[46] V. B. Cheng, H. H. Suzukawa, and M. Wolfsberg, J. Chem. Phys. **59**, 3992 (1973).